ACS APPLIED MATERIALS & INTERFACES

Research Article

www.acsami.org

Si/Ti_2O_3/Reduced Graphene Oxide Nanocomposite Anodes for Lithium-Ion Batteries with Highly Enhanced Cyclic Stability

A Reum Park,[†] Dae-Yong Son,[§] Jung Sub Kim,[∥] Jun Young Lee,[†] Nam-Gyu Park,[†,§] Juhyun Park,[⊥] Joong Kee Lee,[∥] and Pil J. Yoo*[,†,‡]

[†]School of Chemical Engineering, [‡]SKKU Advanced Institute of Nanotechnology (SAINT), and [§]Department of Energy Science, Sungkyunkwan University, Suwon 440-746, Republic of Korea

[∥]Advanced Energy Materials Processing Laboratory, Center for Energy Convergence Research, Korea Institute of Science and Technology (KIST), Seoul 130-650, Republic of Korea

[⊥]School of Chemical Engineering and Materials Science, Chung-Ang University, Seoul 156-756, Republic of Korea

Supporting Information

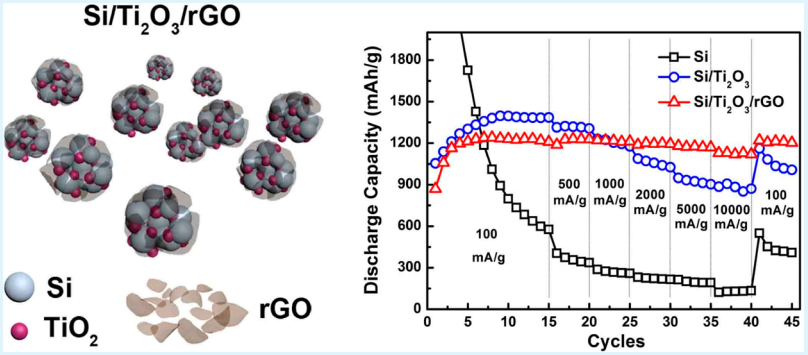

ABSTRACT: Silicon (Si) has attracted tremendous attention as a high-capacity anode material for next generation Li-ion batteries (LIBs); unfortunately, it suffers from poor cyclic stability due to excessive volume expansion and reduced electrical conductivity after repeated cycles. To circumvent these issues, we propose that Si can be complexed with electrically conductive Ti_2O_3 to significantly enhance the reversible capacity and cyclic stability of Si-based anodes. We prepared a ternary nanocomposite of Si/Ti_2O_3/reduced graphene oxide (rGO) using mechanical blending and subsequent thermal reduction of the Si, TiO_2 nanoparticles, and rGO nanosheets. As a result, the obtained ternary nanocomposite exhibited a specific capacity of 985 mAh/g and a Coulombic efficiency of 98.4% after 100 cycles at a current density of 100 mA/g. Furthermore, these ternary nanocomposite anodes exhibited outstanding rate capability characteristics, even with an increased current density of 10 A/g. This excellent electrochemical performance can be ascribed to the improved electron and ion transport provided by the Ti_2O_3 phase within the Si domains and the structurally reinforced conductive framework comprised of the rGO nanosheets. Therefore, it is expected that our approach can also be applied to other anode materials to enable large reversible capacity, excellent cyclic stability, and good rate capability for high-performance LIBs.

KEYWORDS: *silicon, reduced titanium oxide, reduced graphene oxide, lithium-ion batteries, anodes*

INTRODUCTION

Recent developments in high-performance portable electronic devices, electric vehicles, and energy storage systems have generated increased need for next-generation lithium-ion batteries (LIBs) with high energy density and excellent cycling properties.[1] Among the various LIB anode materials available that can meet these requirements, silicon (Si) is regarded as one of the most promising due to its high theoretical capacity (4200 mAh/g), which is ∼10 times greater than that of conventional graphite anodes (372 mAh/g).[2] However, Si anode materials undergo large volume changes (∼300%), which results in structural collapse and poor electrical contacts within the anode structure upon charge−discharge cycling. This eventually leads to drastic capacity fading.[3] To address this issue, Si anodes have been modified with carbonaceous materials, such as amorphous carbon, graphite, carbon nanotubes, and graphene (e.g., reduced graphene oxide, rGO), to suppress the structural change while maintaining good electrical conductivity.[4−7]

In particular, graphene can greatly improve the specific capacity and cyclic reversibility due to its large specific surface area (2630 m^2/g), superior electrical conductivity, and increased Li-ion intercalation capability between its sheet-like structures.[8] Moreover, the intrinsically high mechanical

Received: May 28, 2015
Accepted: August 5, 2015
Published: August 5, 2015

DOI: 10.1021/acsami.5b04652
ACS Appl. Mater. Interfaces 2015, 7, 18483−18490

strength of graphene, combined with its added advantage of structural flexibility, enables this material to assume the role of a buffering matrix to accommodate the volume change of the Si anode.[9−11] However, problems associated with the Si/rGO composite system still remain and limit its practical use as a LIB anode material. For example, during composite preparations that use mechanical mixing or solution-based complexation approaches, it is difficult to ensure uniform distribution of the Si over the surface of the graphene nanosheets due to the insufficient interpenetration capability within the stacked graphene structure.[12−14] Therefore, to form homogeneous, well-mixed composites, high-energy ball milling for an extended period of time is required.[15,16] However, this process occasionally results in the formation of an undesired silicon oxide phase or produces larger agglomerates of the active species, which can undermine the cell performance of LIBs.[17]

As a similar alternative route, Si alloys with Li-inactive metallic elements, such as Ni, Mg, Cu, or TiN, have been investigated in an attempt to enhance the structural stability and electrical conductivity of Si anodes during lithiation−delithiation cycles.[18−21] However, this approach is also limited by the intrinsic reactivity of the metallic species with oxygen under the high-energy ball milling process and can lead to the formation of an oxide layer on the composite surface. This reduces the electrical contact between the electrode and electrolyte. Therefore, it is necessary to develop a novel strategy to acquire composite Si anodes that are appropriately complexed with physically stable and highly conductive materials in order to provide structural stability and maximize the specific capacity.

Additionally, since partially reduced titanium oxides (e.g., Ti_2O_3 and Ti_3O_5) have relatively large electronic conductivity and chemical stability compared to the general form of titania (TiO_2), they are considered as good additive candidates for imparting electrical interconnection and structural stability between the active materials.[22−24] Among these partially reduced titanium oxides, the Ti_2O_3 phase plays a superior role in enhancing the electrochemical activity of the electrode because it exhibits better electrical properties than Ti_3O_5.[25] As a consequence, when it is hybridized with Si, Ti_2O_3 can produce well-interconnected pathways for transporting electrons and Li ions to improve the electrical conductivity, thereby increasing the Li ion diffusivity within the anode.

Here, we present a novel means of synthesizing the nanocomposite of Si/Ti_2O_3/rGO for LIB anodes while simultaneously exhibiting enhanced specific capacity, cyclic stability, and rate capability properties. This ternary nanocomposite is prepared by mechanical blending of Si nanoparticles, TiO_2 nanoparticles, and rGO nanosheets under mild conditions, followed by thermal annealing to create the electroconductive phase of Ti_2O_3 (Ti^{3+}). This conductive phase is formed as a result of the partial reduction of TiO_2 (Ti^{4+}) in the presence of Si and rGO, which act as reducing agents.[26,27] The Ti_2O_3 phase formed inside the Si domains can efficiently alleviate the concerns related to the accumulation of stress caused by volume changes in the Si phase during repeated cycles and also facilitate the enhanced transport of electrons and ions. Furthermore, when rGO nanosheets uniformly encompass the Si matrix, they mitigate the problems of self-aggregation and incomplete electrical contact at the Li-active reaction sites. Therefore, our proposed approach can greatly enhance the electrochemical stability of Si-based anodes and is promising for the development of high performance LIBs.

EXPERIMENTAL SECTION

Materials. Si nanoparticles (<100 μm, synthetic) were purchased from CN vision, Korea. Graphite powder (<20 μm, synthetic), titanium(IV) isopropoxide (97%), acetic acid (≥99.7%), and 2-propanol (anhydrous, 99.5%) were obtained from Sigma-Aldrich. $NaNO_3$ (99.0%) was purchased from Yakuri Pure Chemicals Co. Ltd., Japan. H_2SO_4 (95.0%), $KMnO_4$ (99.3%), H_2O_2 (34.5%), and ethanol (95.0%) were purchased from Samchun Chemical Co. Ltd., Korea. All chemicals were used as received without further purification. In all experiments, deionized water with a resistance of 18.2 MΩ was used.

Synthesis. A solution of 37 mL of titanium(IV) isopropoxide with 10 mL of 2-propanol was slowly added dropwise over 30 min to a stirred mixture of acetic acid (80 mL) and deionized (DI) water (250 mL) at 0 °C. The dispersion was then continuously stirred for about 30 min. The temperature of the solution was increased to 80 °C using an oil bath and reacted for 8 h. It was then heated in a titanium autoclave to 230 °C. After reacting for 12 h, the mixture was left to cool to ambient naturally. The resultant white precipitate was centrifuged and washed vigorously with DI water and ethanol several times, followed by drying at 60 °C. Finally, TiO_2 nanoparticles were obtained.[28,29] GO was synthesized using a modified Hummers' method according to our previous study.[30−32] rGO nanosheets were prepared from GO by thermal reduction in a tube furnace at 800 °C for 1 h under a H_2/Ar (1:3) atmosphere.

To prepare the Si/Ti_2O_3/rGO nanocomposites, first Si and TiO_2 nanoparticles at a mass ratio of 1:1 were mixed in a tungsten carbide vial by mechanical ball milling. This process was performed in a planetary ball milling machine (8000D Dual Mixer/Mill, SPEX Sample Prep) for 30 min, rGO was then added continually to the Si/TiO_2 mixture (80:20 of Si/TiO_2:rGO in weight percent), and the mixed substance was ball milled for 20 min. The resulting ternary composite was annealed at 800 °C for 3 h under Ar atmosphere to induce a partial reduction of TiO_2. For a comparison, the Si/Ti_2O_3 binary composites without rGO were also prepared following the same procedure above. Also, Si/Ti_2O_3/graphite composites were prepared as a control to compare the performance between rGO and conventional carbonaceous material.

Structural and Chemical Characterization. The powder X-ray diffractometer (XRD) (D8 Advance, Bruker, Germany) with Cu Kα radiation (λ = 1.5406 Å) in the 2θ range from 5° to 80° with a step size of 0.02° s^{-1}. Raman spectra were taken using a micro-Raman spectrometer system (ALPHA 300M, WITec, Germany). X-ray photoelectron spectroscopic (XPS) (ESCA 2000 instrument, VG Microtech, U.K.) spectra were measured using an Al Kα radiation using an X-ray source. All binding energy values were aligned with calibrating the C 1s peak at 284.6 eV. To determine the actual amount of rGO in the nanocomposites, thermogravimetric analysis (TGA) (TG/DTA7300, SEICO Inst., Japan) was performed under air at a heating rate of 10 °C min^{-1}. Morphologies of the ternary nanocomposites were observed via field emission scanning electron microscopy (FESEM) (JSM-7600F, JEOL, Japan) and high-resolution transmission electron microscopy (HRTEM) (JEM-2100F, JEOL, Japan).

Electrochemical Measurements. Electrochemical properties of the as-prepared samples were measured using coin cells. For the preparation of the working electrodes, Si/Ti_2O_3/rGO ternary nanocomposites were mixed with conductive carbon black (DB 100) and poly(acrylic acid) (PAA; Mw, 250 000, 35 wt % in H_2O, Aldrich) in ethanol at a mass ratio of 70:15:15 to form a homogeneous slurry with a mortar and pestle. The resultant slurry was then uniformly coated on a Cu foil with a doctor blade and dried at 60 °C under vacuum. The loading mass of the active materials was controlled to be ~1.5 mg/cm^2 with a film thickness of 36 μm. Electrochemical cells were assembled with the composite as the anode, Li metal as the counter electrode, and a microporous polypropylene (PP) (Celgard 2400, Celgard) film as the separator. A 1.3 M $LiPF_6$ solution in a 3:7 (v/v) mixture of ethylene carbonate (EC) and diemethyl carbonate (DMC) was used as the electrolyte. In addition, fluoroethylene carbonate (FEC) was added into the electrolyte as an additive. These

DOI: 10.1021/acsami.5b04652
ACS Appl. Mater. Interfaces 2015, 7, 18483−18490

cells were assembled in a glovebox at a relative humidity of ≤0.5% and galvanostatically charged and discharged in the potential range between 0.0 and 3.0 V (vs Li/Li^+) at current densities ranging from 100 to 10 000 mA/g using a multichannel potentiostat/galvanostat (WMPG 1000, WonATech, Korea). The specific capacity values were estimated based on the total amount of active materials in the electrodes. Cyclic voltammetry was carried out in the potential range between 0.0 and 3.0 V at a scan rate of 0.1 mA/s. To observe the structural change of nanocomposites after cycling, cells were carefully disassembled in a glovebox. The electrode films were then rinsed in DMC for 10 min to remove any residual $LiPF_6$ electrolyte and dried before SEM and TEM analysis. The electronic conductivity of the electrodes was evaluated in the frequency range between 100 kHz and 0.1 Hz using an ac voltage with an amplitude of 10 mV via electrochemical impedance spectroscopy (EIS, CHI6143E, CH Instruments, Inc.).

RESULTS AND DISCUSSION

The synthetic procedure for the $Si/Ti_2O_3/rGO$ nanocomposites is schematically presented in Figure 1. First, Si and TiO_2

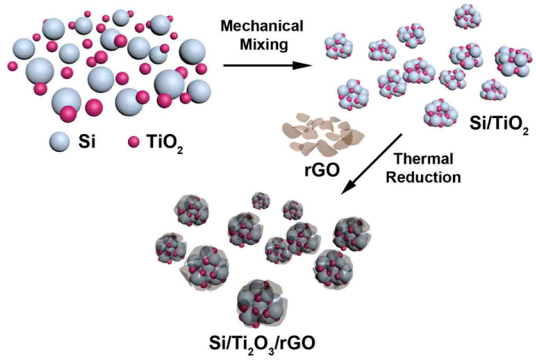

Figure 1. Schematic illustration of the fabrication process for the $Si/Ti_2O_3/rGO$ ternary nanocomposites.

nanoparticles are mixed at a mass ratio of 1:1 via ball milling. At this point, TiO_2 nanoparticles with a smaller diameter (~20 nm) than that of Si (<100 nm) can form a homogeneously complexed phase and prevent the Si nanostructures from growing to microsized grains, as is frequently observed during the intermixing of spherical nanoparticles.[33] Next, rGO nanosheets are added to the prepared Si and TiO_2 mixture; this is followed by additional ball milling to form ternary nanocomposites. Then, to partially reduce TiO_2 to Ti_2O_3 in the presence of Si and carbon (rGO), the samples are annealed at 800 °C for 3 h in an Ar-purged environment.[26,34] The rGO nanosheets used here act as the main reducing agent during the thermal treatment to create the Ti_2O_3 phase from TiO_2. When Ti_2O_3 nanoparticles are uniformly incorporated inside the Si domains, they readily provide stabilized pathways for transporting electrons and Li ion. Thus, this process yields $Si/Ti_2O_3/rGO$ ternary nanocomposites with embedded Ti_2O_3 as an electro-conductive phase.

Crystallographic structures of the as-synthesized nanocomposites were characterized by X-ray diffraction (XRD) measurements (Figure 2). For the composites including both Si and TiO_2, peaks are concurrently observed at 23.8°, 33.1°, 34.8°, 39.6°, 40.2°, 42.6°, 48.8°, 53.8°, 61.3°, 62.4°, 72.4°, and 73.5°, which are assigned to the (012), (104), (110), (006), (113), (202), (024), (116), (214), (300), (1 0 10), and (220) planes of the Ti_2O_3 phase according to JCPDS 89-4746. The characteristic peaks at 28.4°, 47.6°, and 56.1°, which are

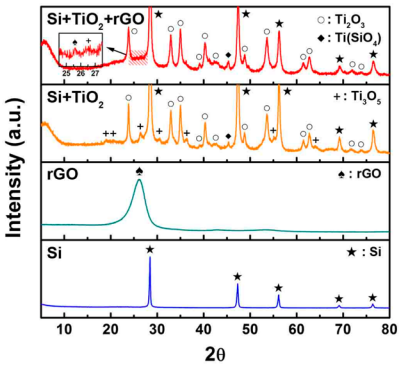

Figure 2. X-ray diffraction patterns for (Si + TiO_2 + rGO), (Si + TiO_2), rGO, and Si (from top to bottom). Composites are named according to their initial composition upon mixing.

assigned to the (111), (220), and (311) planes of Si crystals, are also identified. This confirms the presence of crystalline Si in the composite matrix.[35] Notably, for the case of composites without rGO, additional diffraction peaks at 18.9°, 19.9°, 26.4°, 30.5°, 36.4°, 55.7°, and 64.7° are observed; these can be assigned to the (200), (110), (002), (112), (312), (602), and (204) planes of the Ti_3O_5 phase.[25] This result implies that TiO_2 can be reduced to both Ti_2O_3 and Ti_3O_5 in the presence of only silicon under thermal annealing. Although these reduction reactions proceed simultaneously, the Ti_2O_3 phase is more likely to be produced than Ti_3O_5 (thus, hereafter binary composites will be denoted as Si/Ti_2O_3).[36] However, with the inclusion of rGO for ternary nanocomposites, peaks associated with the Ti_3O_5 phase become significantly weakened in the ternary composites, which is indicative of the successful creation of the Ti_2O_3 phase via a carbothermal reduction process (hereafter ternary composites are denoted as $Si/Ti_2O_3/rGO$). The reduction reactions caused by the presence of rGO are proposed as follows:[26]

$$3TiO_2(s) + C(s) \rightarrow Ti_3O_5(s) + CO(g) \quad (1)$$

$$2Ti_3O_5(s) + C(s) \rightarrow 3Ti_2O_3(s) + CO(g) \quad (2)$$

These observations suggest that the nanocomposite formation in the presence of rGO successfully drives the reduction reaction of TiO_2 to form the Ti_2O_3 phase. Meanwhile, a minor peak corresponding to the $Ti(SiO_4)$ phase was also observed in the composites including both Si and TiO_2.[37] However, since the formation of the Ti_2O_3 phase is dominant in the composites, the influence of the $Ti(SiO_4)$ phase is regarded as negligible in this study.

At the same time, residual rGO nanosheets still act to increase the electrical conductivity by forming interconnections between Si domains. However, it is difficult to clearly capture the rGO peaks in the XRD patterns due to its amorphous character and considerably weaker intensity as compared to the other peaks. As shown in the inset in the uppermost row of Figure 2, the ternary composite showed a very weak peak of rGO ((002) plane) at 25.6°, which is slightly shifted compared to its original position (26.6°) on account of the reestablishment of conjugated graphene network during a complexation with Si/TiO_2 composites.[38]

Raman spectra analysis was conducted to obtain a more detailed understanding of the chemical structure of the $Si/Ti_2O_3/rGO$ nanocomposites, as shown in Figure 3a. The characteristic peaks at 1350 cm^{-1} (D band) and 1580 cm^{-1} (G

DOI: 10.1021/acsami.5b04652
ACS Appl. Mater. Interfaces 2015, 7, 18483−18490

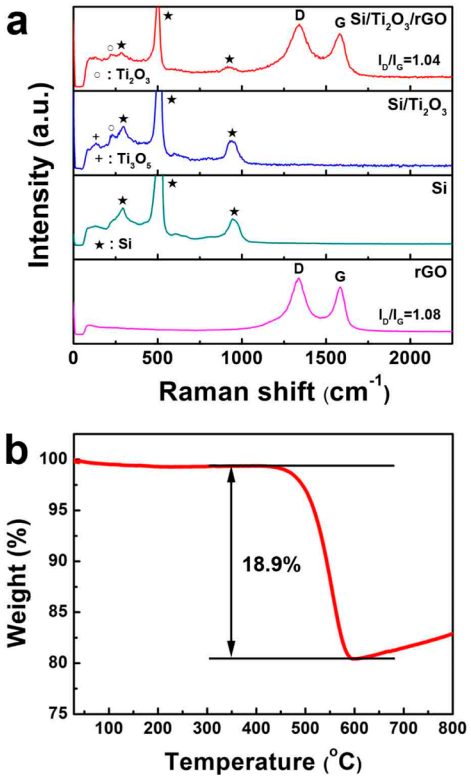

Figure 3. (a) Raman spectra for the $Si/Ti_2O_3/rGO$, Si/Ti_2O_3, Si, and rGO. (b) TGA curve of the $Si/TiO_2/rGO$ under air. Composites are named according to their initial composition upon mixing.

band) are identified as in-plane sp^3 defects and sp^2 domains of the carbon materials, respectively.[39] For the ternary nanocomposites, the intensity ratio of the D and G bands (I_D/I_G) is slightly smaller than that of pure rGO, providing evidence of an increase in the average size of the sp^2 domains during the incorporation of rGO into the Si/TiO_2 binary composites.[40] This also proves the partial reoxidation of RGO as a consequence of reducing TiO_2 to Ti_2O_3. For the Si/Ti_2O_3/rGO ternary nanocomposites, the peak observed at 140 cm^{-1} (corresponding to the Ti_3O_5 phase) is not observed after adding rGO into the binary composite. In addition, the Raman bands at 235 and 295 cm^{-1} (assigned to the Ti_2O_3 and Si phases) are observed; this implies that the TiO_2 phase is mainly converted into Ti_2O_3 without affecting the main structure of the crystalline Si during the complexation process.[25,41] The rGO content in the $Si/Ti_2O_3/rGO$ nanocomposites was determined by thermogravimetric analysis (TGA). As shown in Figure 3b, the mass fraction of rGO in the composite is measured to be 18.9 wt % (20 wt % of rGO is originally mixed into the ternary composites). Therefore, this result indicates that 1.1 wt % of the rGO (5.5% of the initial amount of rGO) has been utilized as a reducing agent for the formation of Ti_2O_3. Meanwhile, the gradual mass increase in the high temperature region of the TGA analysis is ascribed to the oxidation of Si.[42]

In addition, to further characterize the $Si/Ti_2O_3/rGO$ ternary nanocomposites, we investigated the as-synthesized samples using XPS. The survey XPS spectrum (Figure S1) shows that the composite consists of Ti, Si, O, and C. A high resolution O 1s XPS spectrum of Si/Ti_2O_3 binary nanocomposite shows two peaks at 530.0 and 532.5 eV which are attributed to Ti−O and Si−O bonding, respectively.[43,44] However, in the ternary composite, the binding energies of the O 1s of Ti−O and Si−O are observed to be 0.5 and 0.3 eV higher than those in binary composites. This shift of the binding energy of the O 1s electron can be ascribed to the newly created bonding of Ti−O−Si.[45] In addition, the peak at 534.1 eV is assigned for C−OH of rGO.[46] In the XPS spectrum of Ti 2p of the nanocomposites, the binding energies of the Ti $2p_{3/2}$ and Ti $2p_{1/2}$ peaks are observed at 458.6−459.0 eV and 464.2−464.6 eV, respectively, which are in good agreement with the Ti_2O_3 phase.[43] In the absence of rGO, the peaks at 457.0 and 462.5 eV appeared, also due to the occurrence of Ti $2p_{3/2}$ and Ti $2p_{1/2}$ doublet from Ti_3O_5 phase.[47] Another peak observed at 460.5 eV is originated from the $Ti(SiO_4)$ phase.[48] Accordingly, these results are fully consistent with XRD data.

The morphology of the $Si/Ti_2O_3/rGO$ nanocomposites was further elucidated using scanning electron microscopy (SEM). As shown in Figure 4a,b, when Si and TiO_2 nanoparticles are complexed by ball milling and subsequent thermal annealing in the absence of rGO nanosheets, they form agglomerated particles with relatively smooth surfaces. However, when ternary composites are formed, the initially mixed TiO_2 nanoparticles are much smaller than the Si particles and can be uniformly incorporated within the Si domain. Therefore, the formation of large, agglomerated particles can be substantially suppressed. Also, upon introduction of the rGO nanosheets into the binary nanocomposites, the reduction of TiO_2 to Ti_2O_3 is greatly facilitated. As a result, Figure 4c,d shows that uniformly complexed nanocomposites of $Si/Ti_2O_3/rGO$ with fine textures are generated. Energy dispersive X-ray spectroscopic (EDX) mapping with lower magnification shown in panels b−e of Figure S2 demonstrate a homogeneous distribution of each element inside the composite. Since the incorporation of rGO nanosheets inside the binary mixture matrix can greatly enhance the electrical interconnections between Li-active domains, the ternary nanocomposite system is expected to exhibit superior electrochemical performance when used as a LIB anode.

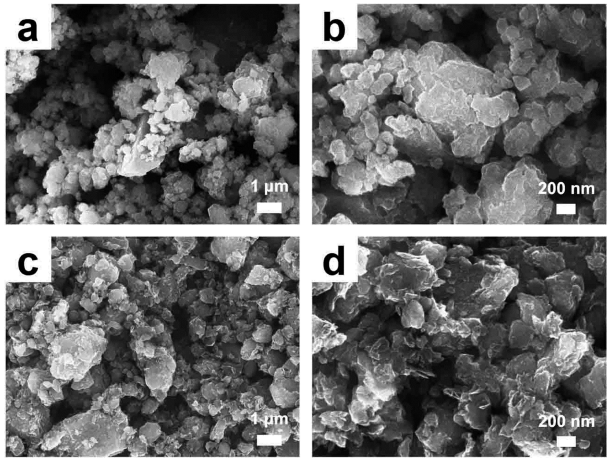

Figure 4. Comparative SEM images of (a, b) Si/Ti_2O_3 binary nanocomposites and (c, d) $Si/Ti_2O_3/rGO$ ternary nanocomposites.

High-resolution transmission electron microscopy (HR-TEM) images reveal the detailed morphologies and crystallinity of the $Si/Ti_2O_3/rGO$ ternary nanocomposites. As shown in Figure 5a, the Si/TiO_2 nanoparticles are wrapped with multilayered rGO nanosheets, indicative of the formation of a homogeneous ternary nanocomposite. In addition, Figure 5b shows that the ternary composite has a lattice fringe spacing of

DOI: 10.1021/acsami.5b04652
ACS Appl. Mater. Interfaces 2015, 7, 18483−18490

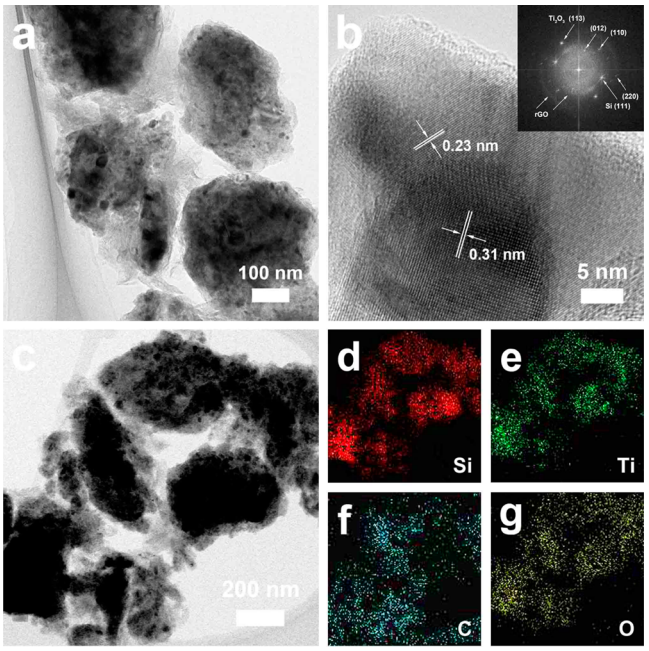

Figure 5. (a) TEM image of the Si/Ti_2O_3/rGO ternary nanocomposites. (b) HRTEM image of part a and FFT analysis (inset). (c) TEM image of the ternary nanocomposite selected for EDX mapping of (d) Si, (e) Ti, (f) C, and (g) O.

0.23 nm, which corresponds to the (113) crystal plane of Ti_2O_3. More importantly, the observed lattice spacing of 0.31 nm, which corresponds to the (111) plane of Si, verifies the intactness of Li-active Si domains, even after the complexation process. The existence of the Ti_2O_3 phase is further proven by fast Fourier transform (FFT) analysis, as shown in the inset of Figure 5b, where the (113), (012), and (110) planes of Ti_2O_3 are indexed. The FFT image also shows the characteristic electron diffraction ring associated with rGO.[49] Along with these crystallographic characterizations, the presence of Si, Ti, C, and O species in the ternary nanocomposites is confirmed by EDX. EDX analysis indicates that the uniformly distributed Si/Ti_2O_3 composite particles are encompassed by the rGO matrix, as shown in the panels d–g of Figure 5.

The electrochemical performances of the Si/Ti_2O_3/rGO nanocomposites as LIB anodes were investigated with cyclic voltammetry (CV) and galvanostatic charging–discharging measurements. CV of the ternary nanocomposites was carried out between the first and tenth cycles in the voltage range between 0.0 and 3.0 V (vs Li^+/Li) at a sweep rate of 0.1 mV/s, as shown in Figure 6a. Cathodic peaks at 0.051 and 0.19 V, which are associated with the lithiation of Si, gradually become apparent due to the slow activation process of the electrode. In the anodic scan, two peaks at 0.35 and 0.49 V are ascribed to the delithiation of Si.[50,51] Notably, the Ti_2O_3 phase is known to react with Li^+ ions via the intercalation process over charge–discharge cycles.[43] However, it is rarely identified with characteristic peaks in the CV curves due presumably to overlapping with relatively intense peaks generated from Si-involved reactions. Therefore, to elucidate the electrochemical properties of the Ti_2O_3 phase in the ternary nanocomposites, XRD patterns were obtained from disassembled cells after the

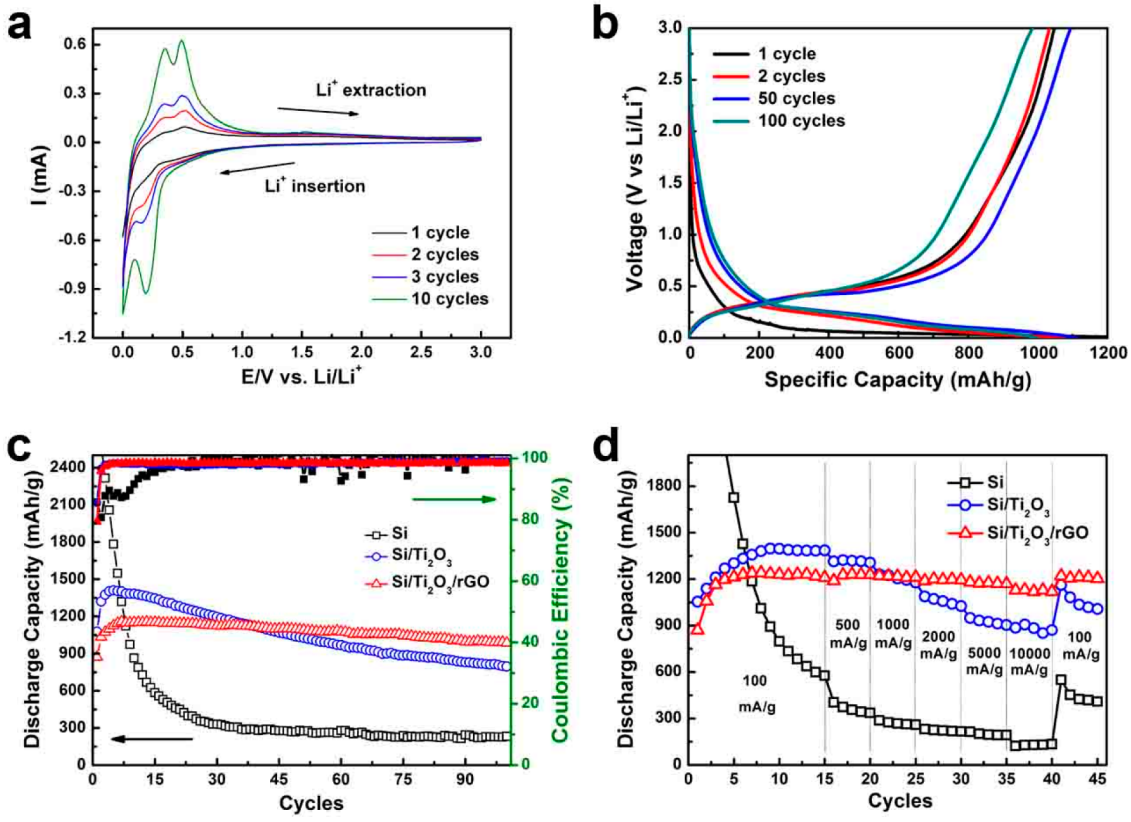

Figure 6. Electrochemical performances of Si/Ti_2O_3/rGO ternary nanocomposite anodes: (a) cyclic voltammetry, (b) galvanostatic charge–discharge profiles at a current density of 100 mA/g, (c) cycling performance and Coulombic efficiency of ternary nanocomposite electrodes during 100 cycles at 100 mA/g, and (d) rate capabilities of ternary nanocomposite electrodes.

DOI: 10.1021/acsami.5b04652
ACS Appl. Mater. Interfaces 2015, 7, 18483–18490

first and second cycles of charge and discharge (Figure S3). Two peaks emerged at 43.0 and 50.2° that originated from the Cu foil. As shown in Figure S3, all peaks associated with Si are significantly weakened by the alloying reaction with Li to form Li_xSi after the first discharge cycle. On the contrary, peaks associated with the Ti_2O_3 phase (black dotted lines) remain unchanged even after subsequent cycles, indirectly implying the occurrence of intercalation/deintercalation of Li ions.[43]

Galvanostatic charge−discharge profiles of $Si/Ti_2O_3/rGO$ nanocomposites were obtained at a current density of 100 mA/g between 0.0 and 3.0 V versus Li^+/Li, as shown in Figure 6b. In the first charging curve, the long plateau observed between 0.01 and 0.1 V implies the formation of an amorphous Li_xSi phase. Alternatively, in the discharging process, the delithiation peak of Li_xSi alloys is observed at 0.45 V.[52,53] The initial charge and discharge capacities of the ternary nanocomposites are measured to be 1097 and 871 mAh/g, respectively, leading to a Coulombic efficiency of 79.4%. This irreversible capacity loss can mainly be attributed to the formation of solid electrolyte interphase (SEI) layers between the electrode and electrolyte in the first lithiation process.[54] Additionally, the cycling performance of the ternary nanocomposites is compared with those for Si and Si/TiO_2 binary composites, as shown in Figure 6c. As expected, the Si electrode exhibits rapid capacity fading, down to 7.8% of the initial capacity, after 100 cycles. In the case of Si/Ti_2O_3 binary nanocomposites, the initial charge−discharge capacities are 1259 and 1077 mAh/g, respectively, resulting in a Coulombic efficiency of 85.5%. For the binary composites, the formation of a large amount of Ti_2O_3 enhances the electrical interconnections between Si domains and effectively alleviates the volume expansion of active materials, resulting in a capacity retention of approximately 74% after 100 cycles. When rGO nanosheets are also incorporated into these binary composites, a significant improvement in the conductivity and stability of the electrode is expected. As a result, these devices show charge−discharge capacities of 1001 and 985 mAh/g, respectively, after 100 cycles (with a Coulombic efficiency of 98.4%) and demonstrate excellent reversible characteristics. In addition, obtained result can be compared with the performance from other Si/rGO composite anodes which are similarly prepared by mechanical mixing, in which the capacity retention after 30 cycles is about 83% of the initial discharge capacity of 2753 mAh/g.[12] However, particularly in this study, discharge capacity rarely changes even after 100 cycles. This discerned performance in the cyclic stability might be originated from the efficient inclusion of both electro-conductive and Li-intercalation-capable Ti_2O_3 phase in the ternary nanocomposites.

Furthermore, in order to understand the contribution of Ti_2O_3 and rGO phases for the enhanced electrochemical performances, we varied the composition ratio in the ternary nanocomposites and observed charge−discharge characteristics (Figure S4). As shown, upon increasing the amount of Ti_2O_3 phase (30:50:20 (w/w) mixture of $Si/Ti_2O_3/rGO$), a relative decrease in the Li-reactive Si phase undermines the overall capacity, though it still retains good cyclic stability. Meanwhile, when the amount of rGO inclusion is decreased (45:45:10 (w/w) mixture of $Si/Ti_2O_3/rGO$), the obtained capacity falls short of the expected performance notwithstanding an increase in the amount of Li-active species of Si and Ti_2O_3, implying the crucial role of rGO nanosheet interconnections for the enhanced conductivity and resulting high capacity characteristics. Also, for a comparison, rGO is replaced with conventional graphite and the performance of Si/Ti_2O_3/graphite ternary nanocomposites is also evaluated. As expected, nonexfoliated graphite provides less interconnected matrix and incomplete interfacial contact with Si and Ti_2O_3 domains, thus, it results in inferior performance in the reversible capacity and cyclic stability. The electrodes also exhibit outstanding rate capability characteristics at various current densities, as shown in Figure 6d. The rate performance is evaluated at current densities ranging from 100 to 10 000 mA/g. To our surprise, in the case of the $Si/Ti_2O_3/rGO$ ternary nanocomposites, the specific capacity rarely changes, even when a high current density of 10 000 mA/g is applied. Moreover, the capacity value is soon recovered to 1202 mAh/g when the current density is switched to 100 mA/g.

To further elucidate the electrochemical performance of the $Si/Ti_2O_3/rGO$ nanocomposites, electrochemical impedance spectra (EIS) analysis was carried out. The Nyquist plots of cells with electrodes that have been cycled 100 times were observed, as shown in Figure 7. The entire plot is comprised of

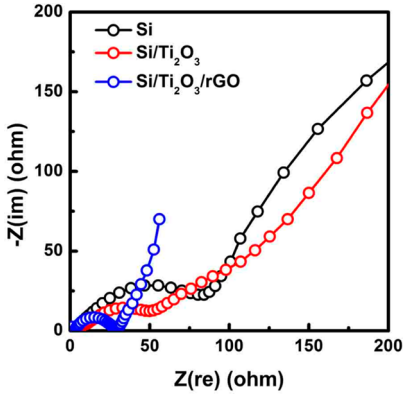

Figure 7. EIS plots of Si, Si/Ti_2O_3, and $Si/Ti_2O_3/rGO$ nanocomposites after 100 cycles.

one semicircle in the high frequency region and an inclined line in the low frequency region; these features can be assigned to the charge-transfer resistance and diffusion resistance of the electrode materials, respectively.[55] The diameter of the semicircle for the ternary nanocomposites appears to be much smaller than those of the binary nanocomposites and Si, thereby implying that the $Si/Ti_2O_3/rGO$ composite has the lowest resistance during the interfacial electrochemical reactions; this is also explained by the excellent rate capability of the ternary nanocomposites. Therefore, through the incorporation with TiO_2 and the subsequent reduction reaction to Ti_2O_3, the rGO nanosheets effectively enhance the conductivity and the stability of Si-based electrodes. In addition, the structural stability of $Si/Ti_2O_3/rGO$ ternary nanocomposites is confirmed via SEM and TEM after charge−discharge cycles. As shown in Figure 8, the morphologies of the electrodes after one cycle and 100 cycles show no discernible changes. Furthermore, EDX results (Figure S5) reveals the Si/Ti_2O_3 phase is uniformly wrapped with rGO nanosheet even after lithiation−delithiation cycles. Therefore, this suggests a substantial improvement in the structural stability of the ternary nanocomposites.

CONCLUSIONS

In summary, a novel $Si/Ti_2O_3/rGO$ ternary nanocomposite, for use as a Li-ion battery anode, was prepared by incorporating TiO_2 nanoparticles into the Si matrix under the partial

DOI: 10.1021/acsami.5b04652
ACS Appl. Mater. Interfaces 2015, 7, 18483−18490

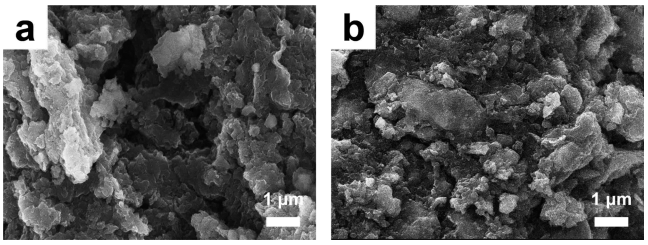

Figure 8. Comparative SEM images of the internal structure of Si/Ti_2O_3/rGO ternary nanocomposite electrodes (a) after one cycle and (b) after 100 cycles.

reduction reaction conditions of thermal annealing using rGO as the reducing agent. The resultant electro-conductive Ti_2O_3 phase effectively alleviated the problems associated with the volumetric change of the Si anodes upon cycling and provided stable electrical interconnection between the active materials. Moreover, rGO nanosheets uniformly encompassed the composites to enhance the specific capacity and cycling stability of the anodes due to their good structural flexibility and electrical conductivity. As a result, Si/Ti_2O_3/rGO ternary nanocomposites can achieve a stable, reversible capacity of 985 mAh/g with good Coulombic efficiency after 100 cycles (98.4%). Also, the resulting anodes showed a substantially high rate capability, even when the applied current density increased to 10 A/g. Because of its notable electrochemical performances, the synthesized Si/Ti_2O_3/rGO ternary nanocomposite in this study is a promising anode material. Further manipulation and optimization should enable the extension of this strategy to other materials for a variety of high-performance energy storage applications.

■ ASSOCIATED CONTENT

Supporting Information

The Supporting Information is available free of charge on the ACS Publications website at DOI: 10.1021/acsami.5b04652.

XPS, SEM, XRD, rate capabilities, and TEM data (PDF)

■ AUTHOR INFORMATION

Corresponding Author

*E-mail: pjyoo@skku.edu.

Notes

The authors declare no competing financial interest.

■ ACKNOWLEDGMENTS

This work was supported by research grants of NRF (Grants 2012M1A2A2671795, 2014M3A7B4052200, and 2014M3C1A3053035) and Basic Science Research Program (Grant 2010-0027955) funded by the National Research Foundation under the Ministry of Science, ICT & Future, Korea.

■ REFERENCES

(1) Tarascon, J.-M.; Armand, M. Issues and Challenges Facing Rechargeable Lithium Batteries. *Nature* **2001**, *414*, 359−367.

(2) Obrovac, M. N.; Christensen, L. Structural Changes in Silicon Anodes during Lithium Insertion/Extraction. *Electrochem. Solid-State Lett.* **2004**, *7*, A93−A96.

(3) Yang, J.; Wang, B. F.; Wang, K.; Liu, Y.; Xie, J. Y.; Wen, Z. S. Si/C Composites for High Capacity Lithium Storage Materials. *Electrochem. Solid-State Lett.* **2003**, *6*, A154−A156.

(4) Datta, M. K.; Maranchi, J.; Chung, S. J.; Epur, R.; Kadakia, K.; Jampani, P.; Kumta, P. N. Amorphous Silicon−Carbon based Nanoscale Thin Film Anode Materials for Lithium Ion Batteries. *Electrochim. Acta* **2011**, *56*, 4717−4723.

(5) Zhang, T.; Gao, J.; Fu, L. J.; Yang, L. C.; Wu, Y. P.; Wu, H. Q. Natural Graphite Coated by Si Nanoparticles as Anode Materials for Lithium Ion Batteries. *J. Mater. Chem.* **2007**, *17*, 1321−1325.

(6) Wang, W.; Kumta, P. N. Nanostructured Hybrid Silicon/Carbon Nanotube Heterostructures: Reversible High-Capacity Lithium-Ion Anodes. *ACS Nano* **2010**, *4*, 2233−2241.

(7) Yang, S.; Li, G.; Zhu, Q.; Pan, Q. Covalent Binding of Si Nanoparticles to Graphene Sheets and its Influence on Lithium Storage Properties of Si Negative Electrode. *J. Mater. Chem.* **2012**, *22*, 3420−3425.

(8) Yoo, E.; Kim, J.; Hosono, E.; Zhou, H.; Kudo, T.; Honma, I. Large Reversible Li Storage of Graphene Nanosheet Families for Use in Rechargeable Lithium Ion Batteries. *Nano Lett.* **2008**, *8*, 2277−2282.

(9) Ji, J.; Ji, H.; Zhang, L. L.; Zhao, X.; Bai, X.; Fan, X.; Zhang, F.; Ruoff, R. S. Graphene-Encapsulated Si on Ultrathin-Graphite Foam as Anode for High Capacity Lithium-Ion Batteries. *Adv. Mater.* **2013**, *25*, 4673−4677.

(10) Gao, X.; Li, J.; Xie, Y.; Guan, D.; Yuan, C. A Multilayered Silicon-Reduced Graphene Oxide Electrode for High Performance Lithium-Ion Batteries. *ACS Appl. Mater. Interfaces* **2015**, *7*, 7855−7862.

(11) Xu, B.; Wu, H.; Lin, C. X.; Wang, B.; Zhang, Z.; Zhao, X. S. Stabilization of Silicon Nanoparticles in Graphene Aerogel Framework for Lithium Ion Storage. *RSC Adv.* **2015**, *5*, 30624−30630.

(12) Xiang, H.; Zhang, K.; Ji, G.; Lee, J. Y.; Zou, C.; Chen, X.; Wu, J. Graphene/Nanosized Silicon Composites for Lithium Battery Anodes with Improved Cycling Stability. *Carbon* **2011**, *49*, 1787−1796.

(13) Park, S.; Kim, H.; Ahn, D.; Lee, S.; Roh, K. C.; Kim, K. Self-assembly of Si Entrapped Graphene Architecture for High-Performance Li-ion Batteries. *Electrochem. Commun.* **2013**, *34*, 117−120.

(14) Yi, R.; Zai, J.; Dai, F.; Gordin, M. L.; Wang, D. Dual Conductive Network-Enabled Graphene/Si−C Composite Anode with High Areal Capacity for Lithium-ion Batteries. *Nano Energy* **2014**, *6*, 211−218.

(15) Noh, H. K.; Park, H.-S.; Jeong, H. Y.; Lee, S. U.; Song, H.-K. Doubling the Capacity of Lithium Manganese Oxide Spinel by a Flexible Skinny Graphitic Layer. *Angew. Chem., Int. Ed.* **2014**, *53*, 5059−5063.

(16) Wang, D.; Gao, M.; Pan, H.; Wang, J.; Liu, Y. High Performance Amorphous-Si@SiO_x/C Composite Anode Materials for Li-ion Batteries derived from Ball-milling and in situ Carbonization. *J. Power Sources* **2014**, *256*, 190−199.

(17) Lee, H.-Y.; Lee, S.-M. Carbon-coated Nano-Si Dispersed Oxides/Graphite Composites as Anode Material for Lithium Ion Batteries. *Electrochem. Commun.* **2004**, *6*, 465−469.

(18) Wang, G. X.; Sun, L.; Bradhurst, D. H.; Zhong, S.; Dou, S. X.; Liu, H. K. Nanocrystalline NiSi Alloy as an Anode Material for Lithium-Ion Batteries. *J. Alloys Compd.* **2000**, *306*, 249−252.

(19) Roberts, G. A.; Cairns, E. J.; Reimer, J. A. Magnesium Silicide as a Negative Electrode Material for Lithium-ion Batteries. *J. Power Sources* **2002**, *110*, 424−429.

(20) Zuo, P.; Yin, G.; Hao, X.; Yang, Z.; Ma, Y.; Gao, Z. Synthesis and Electrochemical Performance of Si/Cu and Si/Cu/graphite Composite Anode. *Mater. Chem. Phys.* **2007**, *104*, 444−447.

(21) Tang, D.; Yi, R.; Gordin, M. L.; Melnyk, M.; Dai, F.; Chen, S.; Song, J.; Wang, D. Titanium Nitride Coating to Enhance the Performance of Silicon Nanoparticles as a Lithium Ion Battery Anode. *J. Mater. Chem. A* **2014**, *2*, 10375−10378.

(22) Tominaka, S.; Tsujimoto, Y.; Matsushita, Y.; Yamaura, K. Synthesis of Nanostructured Reduced Titanium Oxide: Crystal Structure Transformation Maintaining Nanomorphology. *Angew. Chem.* **2011**, *123*, 7556−7559.

(23) Tominaka, S.; Yoshikawa, H.; Matsushita, Y.; Cheetham, A. K. Topotactic Reduction of Oxide Nanomaterials: Unique Structure and

DOI: 10.1021/acsami.5b04652
ACS Appl. Mater. Interfaces 2015, 7, 18483−18490

Electronic Properties of Reduced TiO_2 Nanoparticles. *Mater. Horiz.* **2014**, *1*, 106−110.
(24) Zhong, Y.; Yue, C.; Chen, B.; Sun, S.; Zheng, M.; Zhao, L.; Wu, S.; Li, J.; Kang, J.; Lin, L. Synthetic Preparation of Novel 3D Si/TiO_2−Ti_2O_3 Composite Nanorod Arrays as Anodes in Lithium Ion Batteries. *RSC Adv.* **2015**, *5*, 37399−37404.
(25) Chen, Y.; Mao, J. Sol−gel Preparation and Characterization of Black Titanium Oxides Ti_2O_3 and Ti_3O_5. *J. Mater. Sci.: Mater. Electron.* **2014**, *25*, 1284−1288.
(26) Jha, A.; Yoon, S. J. Formation of Titanium Carbonitride Phases via the Reduction of TiO_2 with Carbon in the Presence of Nitrogen. *J. Mater. Sci.* **1999**, *34*, 307−322.
(27) Kwon, H.; Kang, S. Carbothermal Reduction of Titanium Monoxide (TiO). *J. Ceram. Soc. Jpn.* **2008**, *116*, 1154−1158.
(28) Park, N.-G.; van de Lagemaat, J.; Frank, A. J. Comparison of Dye-Sensitized Rutile- and Anatase-Based TiO_2 Solar Cells. *J. Phys. Chem. B* **2000**, *104*, 8989−8994.
(29) Zaban, A.; Ferrere, S.; Sprague, J.; Gregg, B. A. pH-Dependent Redox Potential Induced in a Sensitizing Dye by Adsorption onto TiO_2. *J. Phys. Chem. B* **1997**, *101*, 55−57.
(30) Park, J. S.; Cho, S. M.; Kim, W.-J.; Park, J.; Yoo, P. J. Fabrication of Graphene Thin Films Based on Layer-by-Layer Self-Assembly of Functionalized Graphene Nanosheets. *ACS Appl. Mater. Interfaces* **2011**, *3*, 360−368.
(31) Sher Shah, Md. S. A.; Park, A. R.; Zhang, K.; Park, J. H.; Yoo, P. J. Green Synthesis of Biphasic TiO_2−Reduced Graphene Oxide Nanocomposites with Highly Enhanced Photocatalytic Activity. *ACS Appl. Mater. Interfaces* **2012**, *4*, 3893−3901.
(32) Park, A. R.; Kim, J. S.; Kim, K. S.; Zhang, K.; Park, J.; Park, J. H.; Lee, J. K.; Yoo, P. J. Si−Mn/Reduced Graphene Oxide Nanocomposite Anodes with Enhanced Capacity and Stability for Lithium-Ion Batteries. *ACS Appl. Mater. Interfaces* **2014**, *6*, 1702−1708.
(33) Zhang, Y.; Zhang, X. G.; Zhang, H. L.; Zhao, Z. G.; Li, F.; Liu, C.; Cheng, H. M. Composite Anode Material of Silicon/Graphite/Carbon Nanotubes for Li-ion Batteries. *Electrochim. Acta* **2006**, *51*, 4994−5000.
(34) Hauf, C.; Kniep, R.; Pfaff, G. Preparation of Various Titanium Suboxide Powders by Reduction of TiO_2 with Silicon. *J. Mater. Sci.* **1999**, *34*, 1287−1292.
(35) Lee, J. K.; Smith, K. B.; Hayner, C. M.; Kung, H. H. Silicon Nanoparticles−Graphene Paper Composites for Li Ion Battery Anodes. *Chem. Commun.* **2010**, *46*, 2025−2027.
(36) Richards, B. S.; Richards, S. R.; Boreland, M. B.; Jamieson, D. N. High Temperature Processing of TiO_2 Thin Films for Application in Silicon Solar Cells. *J. Vac. Sci. Technol., A* **2004**, *22*, 339−348.
(37) Varghese, J.; Joseph, T.; Sebastian, M. T. Sol-Gel Derived $TiSiO_4$ Ceramics for High-k gate Dielectric Applications. *AIP Conf. Proc.* **2011**, *1372*, 193−197.
(38) Willemse, C. M.; Tlhomelang, K.; Jahed, N.; Baker, P. G.; Iwuoha, E. I. Metallo-Graphene Nanocomposite Electrocatalytic Platform for the Determination of Toxic Metal Ions. *Sensors* **2011**, *11*, 3970−3987.
(39) Ferrari, A. C. Raman Spectroscopy of Graphene and Graphite: Disorder, Electron−Phonon Coupling, Doping and Nonadiabatic Effects. *Solid State Commun.* **2007**, *143*, 47−57.
(40) Stankovich, S.; Dikin, D. A.; Piner, R. D.; Kohlhaas, K. A.; Kleinhammes, A.; Jia, Y.; Wu, Y.; Nguyen, S. T.; Ruoff, R. S. Synthesis of Graphene-based Nanosheets via Chemical Reduction of Exfoliated Graphite Oxide. *Carbon* **2007**, *45*, 1558−1565.
(41) Tao, H.-C.; Fan, L.-Z.; Mei, Y.; Qu, X. Self-supporting Si/Reduced Graphene Oxide Nanocomposite Films as Anode for Lithium Ion Batteries. *Electrochem. Commun.* **2011**, *13*, 1332−1335.
(42) Xu, Y.; Zhu, Y.; Wang, C. Mesoporous Carbon/Silicon Composite Anodes with Enhanced Performance for Lithium-ion Batteries. *J. Mater. Chem. A* **2014**, *2*, 9751−9757.
(43) Song, H. J.; Kim, J.-C.; Lee, C. W.; Park, S.; Dar, M. A.; Hong, S.-H.; Kim, D.-W. Reversible Li-storage in Titanium(III) Oxide Nanosheets. *Electrochim. Acta* **2015**, *170*, 25−32.
(44) Stem, N.; de Souza, M. L.; de Faria, D. L. A.; dos Santos Filho, S. G. Formation of Ti(III) and Ti(IV) states in Ti_3O_5 Nano- and Microfibers Obtained from Hydrothermal Annealing of C-Doped TiO_2 on Si. *Thin Solid Films* **2014**, *558*, 67−74.
(45) Zhang, J.; Grabstanowicz, L. R.; Gao, S.; Hosmane, N. S.; Huang, B.; Dai, Y.; Liu, D.-j.; Xu, T. Visible-light Photocatalytic SiO_2-$TiO_{2x}C_x$-C Nanoporous Composites using $TiCl_4$ as the Precursor for TiO_2 and Polyhydroxyl Tannin as the carbon source. *Catal. Sci. Technol.* **2012**, *2*, 390−399.
(46) Yang, D.; Velamakanni, A.; Bozoklu, G.; Park, S.; Stoller, M.; Piner, R. D.; Stankovich, S.; Jung, I.; Field, D. A.; Ventrice, C. A., Jr.; Ruoff, R. S. Chemical Analysis of Graphene Oxide Films after Heat and Chemical Treatments by X-ray Photoelectron and Micro-Raman Spectroscopy. *Carbon* **2009**, *47*, 145−152.
(47) Park, M.-C.; Ko, K.-C.; Lee, W.-J. The Fabrication and Characteristic for Narrow-band Pass Color-filter Deposited by Ti_3O_5/SiO_2 Multilayer. *J. Korean Oph. Opt. Soc.* **2011**, *16*, 357−362.
(48) Hu, S.; Li, F.; Fan, Z. Preparation of SiO_2-Coated TiO_2 Composite Materials with Enhanced Photocatalytic Activity Under UV Light. *Bull. Korean Chem. Soc.* **2012**, *33*, 1895−1899.
(49) McAllister, M. J.; Li, J.-L.; Adamson, D. H.; Schniepp, H. C.; Abdala, A. A.; Liu, J.; Herrera-Alonso, M.; Milius, D. L.; Car, R.; Prud'homme, R. K.; Aksay, I. A. Single Sheet Functionalized Graphene by Oxidation and Thermal Expansion of Graphite. *Chem. Mater.* **2007**, *19*, 4396−4404.
(50) Hassan, F. M.; Chabot, V.; Elsayed, A. R.; Xiao, X.; Chen, Z. Engineered Si Electrode Nanoarchitecture: A Scalable Postfabrication Treatment for the Production of Next-Generation Li-Ion Batteries. *Nano Lett.* **2014**, *14*, 277−283.
(51) Xu, Y.; Zhu, Y.; Han, F.; Luo, C.; Wang, C. 3D Si/C Fiber Paper Electrodes Fabricated Using a Combined Electrospray/Electrospinning Technique for Li-Ion Batteries. *Adv. Energy Mater.* **2015**, *5*, 1400753.
(52) Tang, H.; Zhang, J.; Zhang, Y. J.; Xiong, Q. Q.; Tong, Y. Y.; Li, Y.; Wang, X. L.; Gu, C. D.; Tu, J. P. Porous Reduced Graphene Oxide Sheet Wrapped Silicon Composite Fabricated by Steam Etching for Lithium-ion Battery Application. *J. Power Sources* **2015**, *286*, 431−437.
(53) Wang, W. L.; Nguyen, V. H.; Jin, E. M.; Gu, H.-B. Si-SnO composite as an Anode Material in Lithium Ion Batteries using Novel Polymer Binder. *Mater. Express* **2013**, *3*, 273−279.
(54) Meng, X.; Deng, D. Core−Shell Ti@Si Coaxial Nanorod Arrays Formed Directly on Current Collectors for Lithium-Ion Batteries. *ACS Appl. Mater. Interfaces* **2015**, *7*, 6867−6874.
(55) Wang, X.; Xiang, Q.; Liu, B.; Wang, L.; Luo, T.; Chen, D.; Shen, G. TiO_2 modified FeS Nanostructures with Enhanced Electrochemical Performance for Lithium-Ion Batteries. *Sci. Rep.* **2013**, *3*, 2007.

DOI: 10.1021/acsami.5b04652
ACS Appl. Mater. Interfaces 2015, 7, 18483−18490